# Adiabatic release measurements in aluminum between 400 and 1200 GPa: Characterization of aluminum as a shock standard in the multimegabar regime

M. D. Knudson, M. P. Desjarlais, and Aurora Pribram-Jones

# Adiabatic release measurements in aluminum between 400-1200 GPa: characterization of aluminum as a shock standard in the multimegabar regime

M.D. Knudson* and M.P. Desjarlais

*Sandia National Laboratories, Albuquerque, New Mexico 87185-1195, USA*

Aurora Pribram-Jones

*Department of Chemistry, University of California, Irvine, California 92697, USA*

## Abstract

Aluminum has been used prolifically as an impedance matching standard in the multimegabar regime (1 Mbar = 100 GPa), particularly in nuclear driven, early laser driven, and early magnetically driven flyer plate experiments. The accuracy of these impedance matching measurements depends upon the knowledge of both the Hugoniot and release or reshock response of aluminum. Here we present the results of several adiabatic release measurements of aluminum from ∼400-1200 GPa states along the principal Hugoniot using full density polymethylpentene (commonly known as TPX), and both ∼190 and ∼110 mg/cc silica aerogel standards. These data were analyzed within the framework of a simple, analytical model that was motivated by a first-principles molecular dynamics investigation into the release response of aluminum, as well as by a survey of the release response determined from several tabular equations of state for aluminum. Combined, this theoretical and experimental study provides a method to perform impedance matching calculations without the need to appeal to any tabular equation of state for aluminum. As an analytical model, this method allows for propagation of all uncertainty, including the random measurement uncertainties and the systematic uncertainties of the Hugoniot and release response of aluminum. This work establishes aluminum for use as a high-precision standard for impedance matching in the multimegabar regime.

# I. INTRODUCTION

The high-pressure equation of state (EOS) of materials is important for various applications ranging from, among others, planetary physics[1–3] to inertial confinement fusion.[4,5] The predominant method of obtaining EOS data in the multimegabar regime (1 Mbar = 100 GPa) is through dynamic shock wave compression. Various techniques have been used to perform such experiments, including chemical-explosive drivers,[6] conventional and modified light gas guns,[7,8] explosively driven striker plates,[9–14] high-intensity lasers,[15–20] magnetically driven flyer plates,[21–25] and nuclear explosions.[26–32] The vast majority of these techniques utilize a relative or impedance matching (IM) method[7,33] to infer the high-pressure response of the material of interest. In this method, the shock response of the unknown material is compared to that of a standard. The EOS of the standard is assumed to be known to the extent that by comparing a kinematic measurement of the unknown material, usually the shock velocity, $U_s$, with that of the standard, the high-pressure response of the unknown material can be determined through the use of the Rankine-Hugoniot conservation equations.[34]

In the past, aluminum has been the foremost IM standard in shock wave experiments. Well characterized through gas gun,[7] explosively driven striker plates,[10,11] magnetically driven flyer plates,[21] and nuclear driven techniques,[26,27,29–31] $U_s$ of aluminum would be used to infer the pressure state of a baseplate upon which a sample of interest was placed. Measurement of $U_s$ of the sample of interest and the known response of aluminum would then allow the shocked state of the sample to be inferred. However, the accuracy of the inferred shock response of the sample of interest depends not only upon the Hugoniot response, but also the reshock or release response, depending upon the sample's relative shock impedance with respect to aluminum. This is particularly true in the multimegabar regime, where the often used reflected Hugoniot (RH) approximation[33] breaks down due to significant entropy and temperature increases associated with large amplitude shock waves.[34] Several examples of the use of aluminum as an IM standard can be found in the literature, including, among others, $\alpha$-quartz,[18] LiF,[15] Be,[32] polyimide,[16] polystyrene,[19] $H_2O$,[17,25] LiD,[29] LiH,[30] $N_2$,[8] and $D_2$.[12–14,20,23] In all of these cases, the sample impedance is less than that of aluminum, and thus the release response is crucial to accurately infer the shock response through the IM technique.

Here we present a detailed study of the release response of aluminum, with the goal of characterizing the use of aluminum as an IM standard for lower-impedance materials in the multimegabar regime. In particular, we set out to develop a simple, analytical model for IM calculations that would not require the use of a particular tabular EOS. Such a method would facilitate not only the IM calculation, but would also simplify the use of Monte Carlo methods for propagation of uncertainties in the inferred results.[35]

This goal was accomplished through both theoretical and experimental investigation of the release of aluminum, similar to that used recently in the characterization of $\alpha$-quartz as a high-precision standard.[36] First-principles molecular dynamics (FPMD) calculations were performed and several tabular EOS models for aluminum[37–42] were analyzed to provide insight into the release behavior. Analysis of the FPMD release calculations and tabular EOS release response led to a model framework that was used as the basis to analyze a series of plate-impact, adiabatic release experiments performed at the Sandia Z machine, similar to the concept used previously to investigate the adiabatic release response of aluminum,[43] and more recently $\alpha$-quartz.[36] Three different low-impedance materials, full density poly-methylpentene (commonly known as TPX), and both ~190 and ~110 mg/cc silica aerogel, were used as standards to determine release states at various pressures along the aluminum release path. The results of these experiments validated the model framework motivated by the FPMD calculations and tabular EOS models, and provided experimentally determined parameters for the model.

As a consistency check, this analytical release model was used to perform IM calculations to infer Hugoniot states of the standards for all of the release experiments. This allowed comparison of the IM results with previous direct impact experiments used to define the standards.[44,45] In all three cases the IM results were found to be very consistent with the direct impact results, lending confidence that the analytical release model can be used over a wide range of pressures along the Hugoniot and a wide range of shock impedances. Finally, this model was used to reanalyze laser driven Hugoniot experiments on liquid deuterium,[20] to illustrate how the model developed here differs from other methods used in the literature to perform IM with aluminum as the standard.

Section II discusses the FPMD calculations and tabular EOS analysis performed to investigate the release behavior of aluminum. Section III describes the results of the plate-impact release experiments. Section IV demonstrates the use of the analytical release model to per-

$_{71}$ form IM calculations of the release experiments and to reanalyze laser driven experiments
$_{72}$ on liquid deuterium. The main findings are summarized in Sec. V.

## $_{73}$ II.   FIRST-PRINCIPLES MOLECULAR DYNAMICS AND TABULAR EQUA-
## $_{74}$ TION OF STATE INVESTIGATION OF THE RELEASE RESPONSE OF ALU-
## $_{75}$ MINUM

$_{76}$     To investigate the release response of aluminum, first-principles molecular dynamics
$_{77}$ (FPMD) calculations were performed using VASP (Vienna *ab-initio* simulation program[46]),
$_{78}$ a plane-wave density functional theory code developed at the Technical University of Vienna.
$_{79}$ We used a method similar to that used recently in an investigation of the release response
$_{80}$ of $\alpha$-quartz.[36] Specifically, the aluminum atoms were represented with projector augmented
$_{81}$ wave (PAW) potentials[47,48] and exchange and correlation was modeled with the Perdew-
$_{82}$ Burke-Ernzerhof (PBE) functional.[49] A total of 108 atoms were included in the supercell,
$_{83}$ with a plane wave cutoff energy of 280 and 650 eV for lower pressure ($P$) and higher $P$
$_{84}$ adiabats, respectively. Simulations were performed in the canonical ensemble, with simple
$_{85}$ velocity scaling as a thermostat, and typically covered a few to several picoseconds of real
$_{86}$ time. We used the Baldereschi mean value point[50] of the supercell for the evaluation of the
$_{87}$ Brillouin zone.

$_{88}$     The release paths were calculated using the method outlined in Ref. 36. In short, we took
$_{89}$ advantage of the fact that at the initial reference state, the isentrope and the Hugoniot have
$_{90}$ a second order contact,[34] which is most easily seen by considering a Taylor series expansion
$_{91}$ of the entropy as a function of volume ($V$). Thus for small $V$ changes the isentrope is well
$_{92}$ approximated by the Hugoniot. We therefore approximated each release path as a series of
$_{93}$ small Hugoniot jumps, where each calculated Hugoniot state along the approximated release
$_{94}$ path served as the initial reference state for the subsequent Hugoniot calculation. Typical
$_{95}$ $V$ jumps were of the order of 5%, resulting in $P$ jumps of ~5-10%, with a total of ~12-15
$_{96}$ individual calculations per release path. More details can be found in Ref. 36.

$_{97}$     A release path calculated in this way from ~900 GPa is shown as the green line in Fig. 1.
$_{98}$ Also shown for comparison (black line) is a reflection of the aluminum principal Hugoniot
$_{99}$ about the particle velocity ($u_p$) of the shocked state (see Table I). This so-called reflected
$_{100}$ Hugoniot (RH) is often times used to approximate the release path in the $P - u_p$ plane.[33]
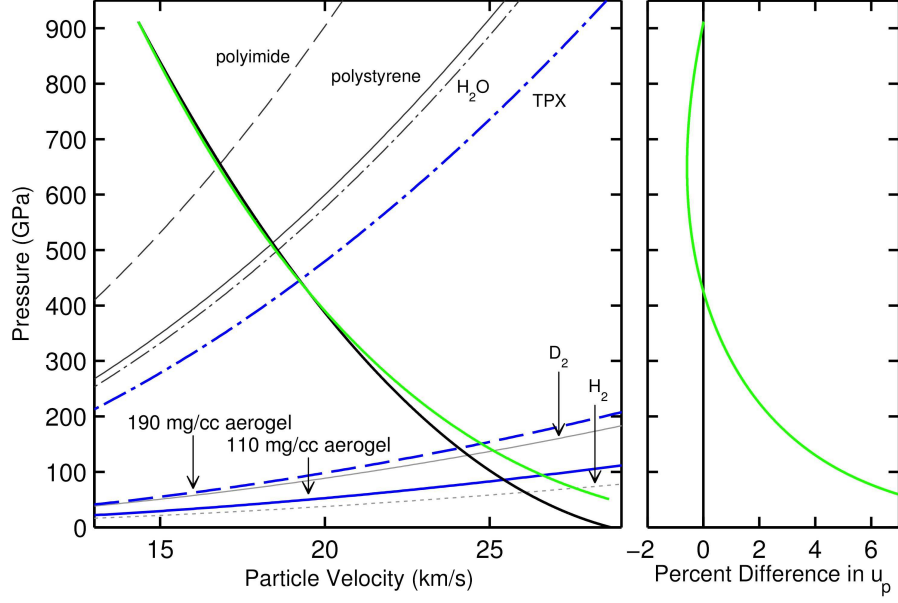
4

FIG. 1. Comparison of the FPMD release path (green) to the RH (black). Also shown are the Hugoniots of polyimide (dashed dark gray), polystyrene (solid dark gray), $H_2O$ (dot-dashed dark gray), $D_2$ (solid light gray), $H_2$ (dotted light gray), TPX (dot-dashed blue), 190 mg/cc aerogel (dashed blue), and 110 mg/cc aerogel (solid blue). The right panel shows the particle velocity residual of the FPMD release with respect to the RH.

The right panel of Fig. 1 shows a useful metric, the particle velocity residual, defined to be the percent difference in particle velocity of the FPMD release with respect to the RH. At low stress or $P$ states on the principal Hugoniot, the RH approximation is reasonably good; recall that the isentrope and Hugoniot have a second order contact. However, at sufficiently high Hugoniot $P$, the RH approximation breaks down, as can be seen in Fig. 1.

For reference, shown as gray lines in Fig. 1, are Hugoniots for several materials that have been studied in dynamic compression experiments using aluminum as a standard. As can been seen in the right panel of Fig. 1, for moderate impedance materials, such as polyimide, polystyrene, and $H_2O$, the correction to the RH in $u_p$ is $\sim 1\%$ negative, while for low impedance materials, such as $D_2$ and $H_2$ the correction to $u_p$ is significantly larger, $\sim 2\text{-}6\%$, but opposite sign. This is significant given that errors in $u_p$ are magnified by a factor of roughly $(\rho/\rho_0 - 1)$ when expressed in terms of density, $\rho$ (the subscript 0 denotes the initial value), i.e. $\delta\rho/\rho \sim (\rho/\rho_0 - 1)\delta u_p/u_p$. These materials exhibit density compression $(\rho/\rho_0)$ between 3-4 in the multimegabar regime, and thus errors in $\rho$ are 2-3 times larger

5

TABLE I. Aluminum[7,10,11,21,26,27,29–31,51] $U_s - u_p$ coefficients and covariance matrix elements ($U_s = C_0 + Su_p$). Note that in this study we only consider the high-$P$ branch of the aluminum Hugoniot ($u_p > 6.25$ km/s).

| | $C_0$ | $S$ | $\sigma_{C_0}^2$ | $\sigma_S^2$ | $\sigma_{C_0}\sigma_S$ |
|---|---|---|---|---|---|
| | (km/s) | | (x10$^{-3}$) | (x10$^{-3}$) | (x10$^{-3}$) |
| high-$P$ | 6.322 | 1.189 | 53.581 | 0.4196 | $-4.605$ |

than the errors in $u_p$.

In accordance with the previous study on the release response of $\alpha$-quartz,[36] we evaluated the aluminum release curves using a Mie-Grüneisen (MG) model with a linear $U_s - u_p$ Hugoniot response as the reference curve, which we will call the MG, linear reference (MGLR) model. In this model the Grüneisen parameter, $\Gamma = V(dP/dE)_V$, is held constant along a given release path. In the $\alpha$-quartz study, such a model was found to quite accurately reproduce the FPMD calculated release paths along nearly their entirety over a very wide $P$ range. The MGLR model has two parameters; $\Gamma$ and the slope, $S$, of the linear $U_s - u_p$ Hugoniot ($U_s = C_0 + Su_p$) used for the reference curve. Note that for a given value of $S$, which we will denote as $S_1$, there is a unique value of $C_{01}$ that will produce ($P_1, u_{p1}$) along the Hugoniot;

$$C_{01} = \frac{P_1}{\rho_0 u_{p1}} - S_1 u_{p1}. \tag{1}$$

The values of $\Gamma$ and $S$ can be simultaneously optimized to minimize the integral:

$$\int_{P_{\min}}^{P_1} \left[ u_p^{\text{rel}}(P') - u_p^{\text{Calc}}(P') \right]^2 dP' \tag{2}$$

where $u_p^{\text{rel}}$ and $u_p^{\text{Calc}}$ are the particle velocities along the MGLR and the calculated release paths (either from FPMD simulations or a tabular EOS), respectively. These optimizations were performed for a total of three FPMD calculated release paths, as well as 8-10 release paths obtained from several different tabular EOS models for aluminum, including 3700 (Refs. 37,38), 3715 (Refs. 39,40), and 3719 (Refs. 41,42). These release paths emanated from various states along the principal Hugoniot ranging from ∼300-3500 GPa. The results of several of these optimizations are shown in Fig. 2, and the values for $\Gamma$ and $S$ of all the
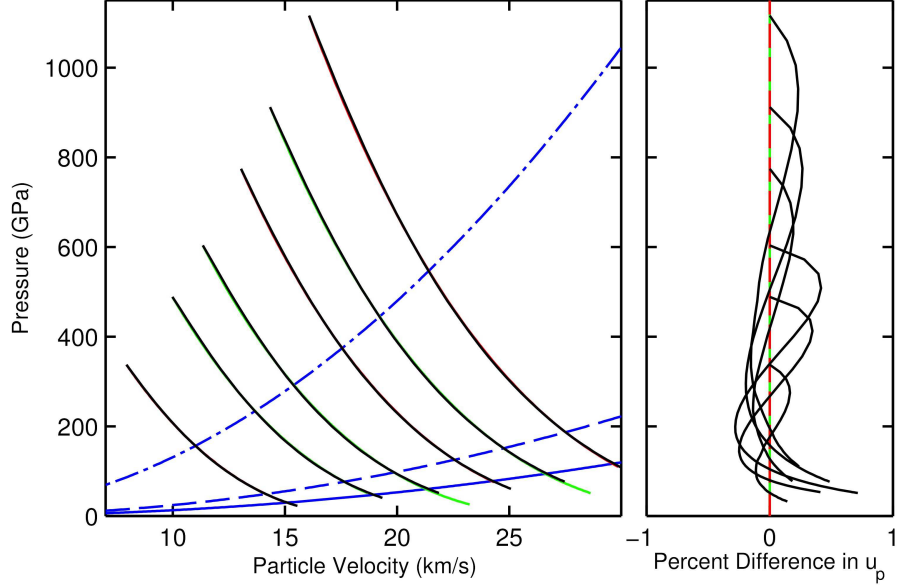
FIG. 2. Comparison of the MGLR release paths (black) with the FPMD release paths (green) and release paths from the 3700 EOS[37,38] (red), each from three different principal Hugoniot states of aluminum. Here both $\Gamma$ and $S$ are optimized for each release path; the values are listed in Tables II and III. Also shown for reference are the Hugoniots for TPX (dot-dashed blue), 190 mg/cc aerogel (dashed blue), and 110 mg/cc aerogel (solid blue). The right panel shows the particle velocity residuals of the MGLR release paths with respect to the FPMD and 3700 release paths. Note the change in scale on the residual plot with respect to Fig. 1.

TABLE II. Values for $\Gamma$ and $S$ for the FPMD release paths using the MGLR model for both cases (i) $\Gamma$ and $S$ optimized, and (ii) $\Gamma$ optimized and $S(u_p^{\mathrm{al}})$ given by Eq. (3).

| $P_{\mathrm{al}}$ | $u_p^{\mathrm{al}}$ | $\Gamma, S$ optimized | | $\Gamma$ optimized | |
|---|---|---|---|---|---|
| (GPa) | (km/s) | $\Gamma$ | $S$ | $\Gamma$ | $S(u_p^{\mathrm{al}})$ |
| 489 | 9.980 | 1.399 | 1.510 | 1.320 | 1.444 |
| 603 | 11.337 | 1.284 | 1.484 | 1.215 | 1.422 |
| 911 | 14.339 | 1.071 | 1.408 | 1.041 | 1.381 |

134 optimizations are displayed in Tables II-V.

135    As can be seen in Fig. 2, the MGLR model is able to reproduce quite well the FPMD and
136 tabular EOS release paths over the entire regime studied here. However, in contrast to the

TABLE III. Values for $\Gamma$ and $S$ for release paths from the 3700 EOS[37,38] using the MGLR model for both cases ($i$) $\Gamma$ and $S$ optimized, and ($ii$) $\Gamma$ optimized and $S(u_p^{\text{al}})$ given by Eq. (3).

| $P_{\text{al}}$ | $u_p^{\text{al}}$ | $\Gamma, S$ optimized | | $\Gamma$ optimized | |
|---|---|---|---|---|---|
| (GPa) | (km/s) | $\Gamma$ | $S$ | $\Gamma$ | $S(u_p^{\text{al}})$ |
| 300.8 | 7.393 | 1.411 | 1.466 | 1.450 | 1.491 |
| 491.6 | 9.985 | 1.188 | 1.411 | 1.232 | 1.444 |
| 599.6 | 11.236 | 1.117 | 1.394 | 1.155 | 1.424 |
| 774.2 | 13.045 | 1.041 | 1.376 | 1.067 | 1.398 |
| 923.6 | 14.438 | 0.995 | 1.364 | 1.012 | 1.379 |
| 1115.9 | 16.073 | 0.962 | 1.359 | 0.963 | 1.360 |
| 1309.7 | 17.587 | 0.935 | 1.357 | 0.921 | 1.344 |
| 1537.3 | 19.226 | 0.900 | 1.350 | 0.879 | 1.328 |

TABLE IV. Values for $\Gamma$ and $S$ for release paths from the 3715 EOS[39,40] using the MGLR model for both cases ($i$) $\Gamma$ and $S$ optimized, and ($ii$) $\Gamma$ optimized and $S(u_p^{\text{al}})$ given by Eq. (3).

| $P_{\text{al}}$ | $u_p^{\text{al}}$ | $\Gamma, S$ optimized | | $\Gamma$ optimized | |
|---|---|---|---|---|---|
| (GPa) | (km/s) | $\Gamma$ | $S$ | $\Gamma$ | $S(u_p^{\text{al}})$ |
| 303.1 | 7.470 | 1.789 | 1.568 | 1.686 | 1.489 |
| 499.2 | 10.156 | 1.398 | 1.515 | 1.312 | 1.441 |
| 602.6 | 11.348 | 1.288 | 1.492 | 1.210 | 1.422 |
| 761.8 | 12.990 | 1.191 | 1.474 | 1.113 | 1.398 |
| 917.3 | 14.448 | 1.146 | 1.475 | 1.054 | 1.379 |
| 1106.1 | 16.072 | 1.108 | 1.473 | 1.001 | 1.360 |
| 1317.8 | 17.744 | 1.042 | 1.445 | 0.955 | 1.342 |
| 2022.8 | 22.568 | 0.882 | 1.364 | 0.831 | 1.301 |
| 2685.6 | 26.386 | 0.745 | 1.306 | 0.719 | 1.276 |
| 3516.5 | 30.553 | 0.602 | 1.222 | 0.635 | 1.256 |

TABLE V. Values for $\Gamma$ and $S$ for release paths from the 3719 EOS[41,42] using the MGLR model for both cases $(i)$ $\Gamma$ and $S$ optimized, and $(ii)$ $\Gamma$ optimized and $S(u_p^{\mathrm{al}})$ given by Eq. 3.

| $P_{\mathrm{al}}$ | $u_p^{\mathrm{al}}$ | $\Gamma, S$ optimized | | $\Gamma$ optimized | |
|---|---|---|---|---|---|
| (GPa) | (km/s) | $\Gamma$ | $S$ | $\Gamma$ | $S(u_p^{\mathrm{al}})$ |
| 306.2 | 7.526 | 1.302 | 1.385 | 1.463 | 1.488 |
| 490.1 | 9.999 | 1.105 | 1.355 | 1.229 | 1.443 |
| 600.6 | 11.277 | 1.035 | 1.338 | 1.148 | 1.423 |
| 771.7 | 13.058 | 0.921 | 1.324 | 1.033 | 1.397 |
| 919.4 | 14.400 | 0.877 | 1.292 | 0.982 | 1.380 |
| 1105.5 | 16.040 | 0.828 | 1.278 | 0.927 | 1.360 |
| 1317.0 | 17.708 | 0.785 | 1.266 | 0.874 | 1.343 |
| 2008.7 | 22.406 | 0.691 | 1.236 | 0.764 | 1.302 |
| 2702.4 | 26.362 | 0.638 | 1.220 | 0.698 | 1.276 |
| 3535.3 | 30.489 | 0.601 | 1.209 | 0.649 | 1.256 |

137 previous $\alpha$-quartz study, where $S$ was found to be essentially independent of the Hugoniot
138 $P$, $S$ was found to decrease monotonically with Hugoniot $P$ in the present aluminum study.
139 This difference in behavior is likely related to the fact that in this regime aluminum is
140 a monatomic, metallic fluid while $\alpha$-quartz is a molecular fluid that exhibits significant
141 disordering and dissociation as the temperature and pressure are increased.[60] It was also
142 found that for a given release path there exists a broad, shallow minimum in the evaluated
143 integral [Eq. (2)] along a line in $\Gamma$-$S$ space, as illustrated in Fig. 3. This broad minimum
144 allowed us to consider prescribing a particular $S(P)$, or more appropriately for the purposes
145 of an IM model, $S(u_p^{\mathrm{al}})$, with only a negligible degradation in the agreement between the
146 MGLR and FPMD release paths; i.e. for a reasonable prescribed value of $S$, a value of $\Gamma$
147 can be found that results in essentially the same minimum for Eq. (2). Since $S$ was found
148 to monotonically decrease with increased Hugoniot $P$, and $S$ appears to asymptote to $\sim$1.2,
149 a value very close to the actual Hugoniot slope (see Table I), we chose to fit the various
150 values of $S$ in Tables II-V to a simple exponential functional form that exhibits this type of

9

TABLE VI. Fit parameters for $S(u_p^{\text{al}})$ [Eq. (3)].

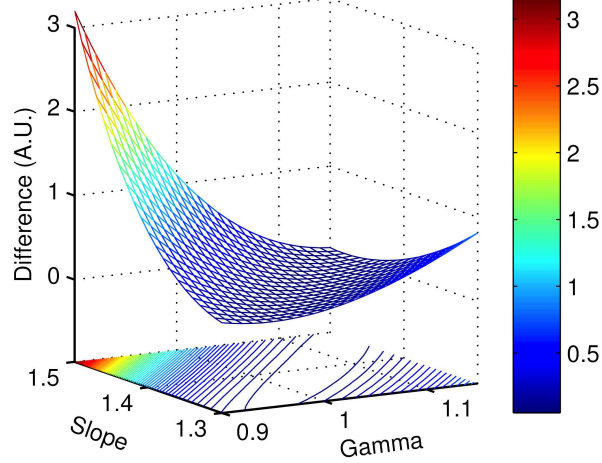| $a_1$ | $a_2$ | $a_3$ |
|-------|-------|-------|
|       |       | $(\text{km/s})^{-1}$ |
| 1.189 | 0.4883 | 0.0652 |



FIG. 3. Integrated difference between the MGLR and the FPMD release paths [Eq. (2)] as a function of both $\Gamma$ and $S$. Note the shallow minimum along a line in $\Gamma$-$S$ space.

151 behavior:

$$S(u_p^{\text{al}}) = a_1 - a_2\text{exp}\left[-a_3u_p^{\text{al}}\right], \tag{3}$$

152 where $a_1$ was fixed to the actual Hugoniot slope of 1.189 (see Table I). The best fit values
153 of the other two free parameters are listed in Table VI.

154     We then repeated the optimization process, this time optimizing only $\Gamma$ while determining
155 $S(u_p^{\text{al}})$ through Eq. (3). The results of this optimization are shown in Fig. 4 and the values
156 of $\Gamma$ and $S(u_p^{\text{al}})$ are displayed in Tables II-V. Comparison of Figs. 2 and 4 indicate that, as
157 expected, simplification in the MGLR model by prescribing $S(u_p^{\text{al}})$ through Eq. (3) results
158 in only a negligible degradation in the agreement between the MGLR and FPMD release
159 paths.

160     $\Gamma$ was also found to have a strong dependence on the Hugoniot $P$. $\Gamma$ is relatively large at
161 low $P$, decreases with increasing $P$, and appears to asymptote to a value of $\sim$0.6. This is
162 very similar to the asymptotic value found on the $\alpha$-quartz study[36] and is quite close to the
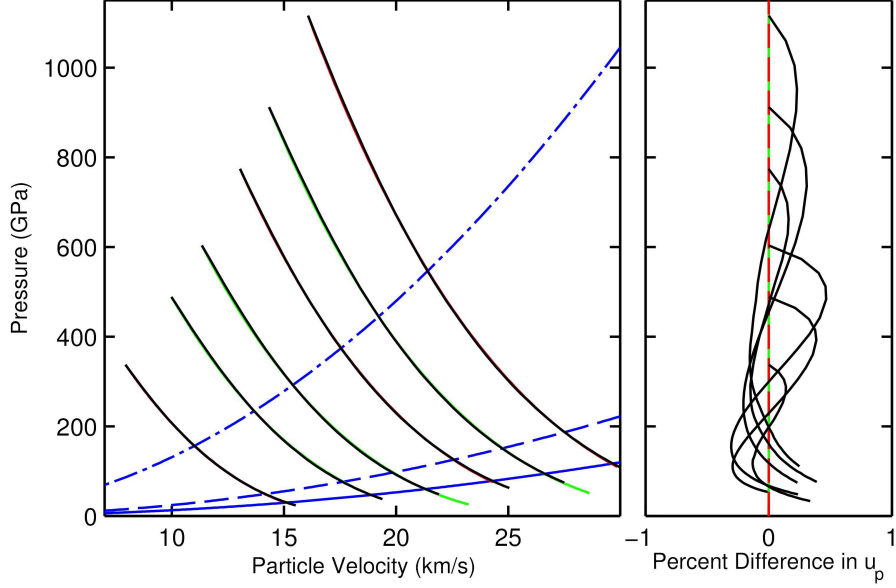
FIG. 4. Comparison of the MGLR release paths (black) with the FPMD release paths (green) and release paths from the 3700 EOS (red), each from three different principal Hugoniot states of aluminum. Here $S(u_p^{\mathrm{al}})$ is given by Eq. (3) and only $\Gamma$ is optimized for each release path; the values are listed in Tables II and III. Also shown for reference are the Hugoniots for TPX (dot-dashed blue), 190 mg/cc aerogel (dashed blue), and 110 mg/cc aerogel (solid blue). The right panel shows the particle velocity residuals of the MGLR release paths with respect to the FPMD and 3700 release paths.

value of 2/3 that one would expect for an ideal gas. As was the case in the $\alpha$-quartz study, the asymptotic behavior of $\Gamma$ and $S$ is quite intriguing. However, it is not clear whether the behaviors of $\Gamma$ and $S$ are the result of underlying physics, or merely a coincidence. To understand this further would require a rather extensive FPMD investigation, which is outside of the scope of this study.

It should be emphasized that the MGLR model discussed here is only intended to calculate kinematic variables for aluminum upon release, in particular the release paths in the $P - u_p$ plane for purposes of impedance matching. For instance, it is anticipated that the temperatures and specific heats of the MGLR model do not reflect the behavior of aluminum in this regime. To underscore this, we choose to refer to $\Gamma$ in the MGLR model as the effective $\Gamma$, or $\Gamma_{\mathrm{eff}}$, from this point forward.

This investigation of the release response of aluminum suggests that from a given alu-

11

TABLE VII. TPX and silica aerogel $U_s - u_p$ coefficients and covariance matrix elements[44,45]

| | $C_0$ | $S$ | $\sigma^2_{C_0}$ | $\sigma^2_S$ | $\sigma_{C_0}\sigma_S$ |
|---|---|---|---|---|---|
| | (km/s) | | (x10$^{-3}$) | (x10$^{-3}$) | (x10$^{-3}$) |
| TPX | 2.691 | 1.310 | 3.667 | 0.0152 | $-0.2155$ |
| 190 mg/cc aerogel | $-0.393$ | 1.248 | 34.17 | 0.100 | $-1.822$ |
| 110 mg/cc aerogel | $-0.703$ | 1.232 | 66.82 | 0.159 | $-3.193$ |

minum Hugoniot state, the release path can be calculated using a MGLR model with a constant $\Gamma_{\text{eff}}$. $\Gamma_{\text{eff}}$ is a function of $P$, or more appropriately for the purposes of an IM model, a function of $u_p^{\text{al}}$ along the aluminum Hugoniot. $S$ of the linear $U_s - u_p$ Hugoniot used as the reference for the MG model is also a function of $u_p^{\text{al}}$, and is given by Eq. (3). $C_{01}$ is then determined through Eq. (1). This model serves as the framework for analysis of the release measurements that will be discussed in the next section.

## III.   EXPERIMENTAL RESULTS AND DISCUSSION

A series of planar, plate-impact, shock wave experiments were performed at the Sandia Z machine[52] to investigate the release response of aluminum, using the experimental configurations described in Ref. 36. Three different low-impedance standards were used to obtain release states from shocked aluminum: polymethylpentene (commonly known as TPX), and both ∼190 and ∼110 mg/cc silica aerogel. The shock response of these standards have been previously investigated on the Z machine.[44,45] Since these samples are solid, they could be directly impacted by the flyer plate, and thus the Hugoniot states could be inferred through simple IM with aluminum under compression, to relatively high-precision. The linear $U_s - u_p$ coefficients and associated uncertainties for these three materials, which were used in the analysis of the release experiments described here, are listed in Table VII.

The aluminum (6061-T6), TPX (obtained from Mitsui Chemicals America), and ∼190 and ∼110 mg/cc silica aerogel (fabricated by General Atomics) samples were all nominally 5 mm in lateral dimension. The thickness of the aluminum was nominally 300 microns, while the thicknesses of the release standards were all nominally 1000 microns. The samples were metrologized using a measuring microscope to determine sample diameters and an

interferometer to measure thickness to a precision of ∼5 microns and less than 1 micron, respectively. Density of the silica aerogel was inferred from high-precision mass measurements and inferred volume assuming the samples were right-circular cylinders. Slight departure from the right-circular cylinder assumption resulted in density uncertainty of ∼2% and ∼5% for the 190 and 110 mg/cc aerogel, respectively.

The aluminum samples and release standards were glued together to form experimental "stacks" using the techniques described in Ref. 36. The flyer plates and experimental "stacks" were diagnosed using a velocity interferometer (VISAR[53]). Since the aluminum is opaque, the 532 nm laser light would pass through the transparent low-impedance standard and reflect off the aluminum/standard interface, as illustrated in the inset of Fig. 5. Shock breakout into the release standard resulted in a 10-100's of GPa shock that was of sufficient magnitude that the release standard became weakly reflecting, allowing direct measure of the shock velocity in the release standard with the VISAR diagnostic. As in the $\alpha$-quartz study, the measured apparent velocity of the shock in the release standards was reduced by a factor equal to the refractive index of the un-shocked material: $v = v_a/n_0$. The values of $n_0$ used in this study for TPX and the ∼190 and ∼110 mg/cc silica aerogel were, 1.46, 1.038, and 1.02 respectively.[44,54–56] Representative velocity profiles are shown in Fig. 5. The inferred shocked state of the aluminum sample relied on flyer plate velocity measurements directly above and below the sample "stack" obtained from the VISAR diagnostic, as illustrated in Fig. 5. The impact velocity was taken to be the average of these two measurements, which typically differed by less than 1%. $u_p^{\mathrm{al}}$ of the shocked state was then 1/2 the impact velocity, as a result of the symmetric impact. Uncertainties in the flyer plate and shock velocities were a few tenths of a percent.

The aluminum release experiments were analyzed within the framework of the MGLR model described in the previous section, which is graphically illustrated in Fig. 6. The measured impact velocity and known Hugoniot of aluminum (fit parameters and uncertainties are listed in Table I) defined the initial state in the $P - u_p$ plane, $(P_1, u_{p1})$. The measured shock velocity and the known Hugoniot of the release standard defined the release state along the aluminum release path, $(P_r, u_{pr})$. The MGLR model, with $S_1$ and $C_{01}$ given by Eqs. (3) and (1), respectively, was then used to determine the value of $\Gamma_{\mathrm{eff}}$ such that the release path emanating from $(P_1, u_{p1})$ went through the point $(P_r, u_{pr})$. Uncertainties in the inferred quantities were determined using the Monte Carlo method described in Ref. 36. Note that
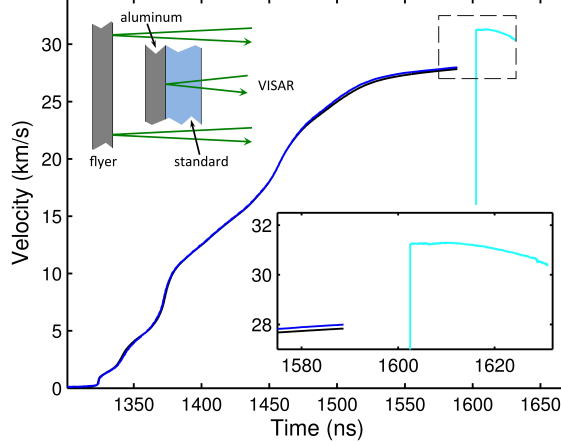
13

FIG. 5. Representative experimental VISAR data. Black (blue) line, aluminum flyer plate velocity below (above) release sample stack; cyan line, release standard shock velocity. The inset shows a schematic of the experimental configuration. Note the dimensions are not to scale.

the uncertainty in $u_{pr}$ that arises from both the uncertainty of the standard Hugoniot and the measured $U_s^{\text{standard}}$ is less than 1%, and provides a tight constraint on the value of $\Gamma_{\text{eff}}$ that connects $(P_1, u_{p1})$ and $(P_r, u_{pr})$. This translates into an uncertainty in $\Gamma_{\text{eff}}$ of between 0.04-0.17 for the individual release measurements.

A total of 7, 7, and 5 aluminum release experiments were performed with TPX, $\sim$190 and $\sim$110 mg/cc silica aerogel, respectively. The pertinent parameters for these experiments are listed in Tables VIII-X. $u_p^{\text{al}}$, $U_s^{\text{standard}}$ and $\rho_0^{\text{standard}}$ denote the measured particle velocity in the aluminum sample, shock velocity in the release standard, and density of the release standard, respectively. $\Gamma_{\text{eff}}$ denotes the inferred value of the effective $\Gamma$ for the MGLR model obtained using the method described above. $u_p^{\text{IM}}$ is the inferred particle velocity in the shocked standard as determined through IM calculations using the MGLR model. These calculations will be discussed in the next section.

The values for $\Gamma_{\text{eff}}$ inferred from all three release standards are plotted as a function of $u_p^{\text{al}}$ in Fig. 7. Also plotted in the figure are the optimized $\Gamma_{\text{eff}}$ obtained from the MGLR model with $S(u_p^{\text{al}})$ given by Eq. (3) that best matched the FPMD release paths and the release paths from various tabular EOS models for aluminum, including 3700 (Refs. 37,38), 3711 (Ref. 57), 3715 (Refs. 39,40), 3719 (Refs. 41,42), and 3720 (Ref. 58). The trend exhibited by the experimentally determined $\Gamma_{\text{eff}}$ is very similar to that exhibited by the FPMD and tabular EOS derived values. Furthermore, the data for all three release standards, which vary by
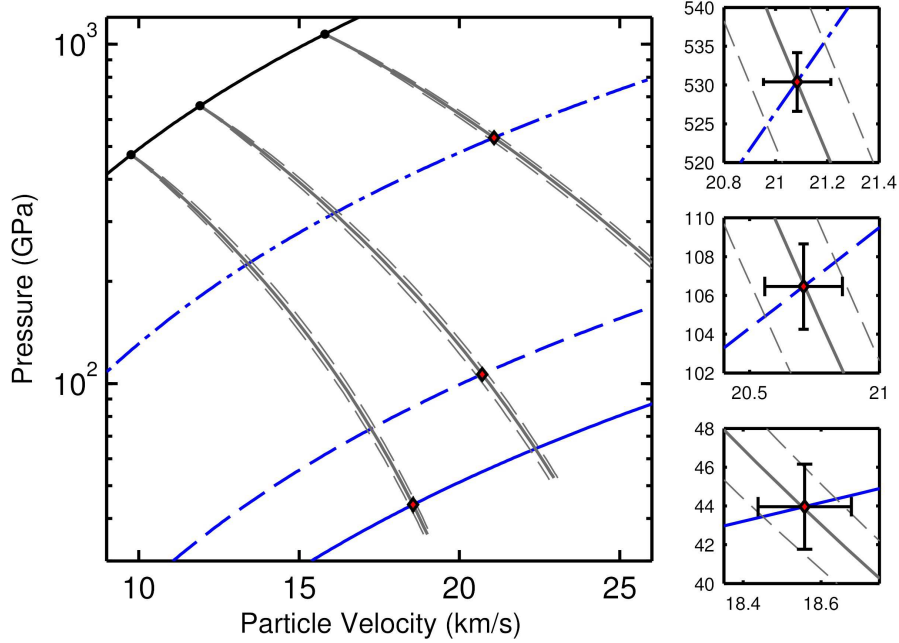
14

FIG. 6. Aluminum release measurements. Black line, aluminum principal Hugoniot; black circles, initial shocked states of aluminum; dot-dashed blue line, TPX Hugoniot; dashed (solid) blue line, 190 mg/cc (110 mg/cc) aerogel Hugoniot; red diamonds, measured release states; solid (dashed) gray lines, release paths for the best fit $\Gamma_{\text{eff}}$ (one-sigma standard deviation). Right panels shown for more detail.

roughly an order of magnitude in shock impedance, all fall along the same trend line. These two observations are a strong indicator that the MGLR framework adequately describes the release response of aluminum in the multimegabar regime over a fairly substantial $P$ range along the Hugoniot and over a wide range of shock impedances.

Just as in the case of the FPMD and tabular EOS derived $\Gamma_{\text{eff}}$, the experimentally determined $\Gamma_{\text{eff}}$ appears to asymptote at high $P$. We therefore fit the experimentally determined $\Gamma_{\text{eff}}$ to a simple exponential functional form that exhibits this type of behavior:

$$\Gamma_{\text{eff}}(u_p^{\text{al}}) = a_1 - a_2 \exp\left[-a_3 u_p^{\text{al}}\right], \tag{4}$$

where $a_1$ was fixed at 0.6, similar to the asymptotic value that was observed in the $\alpha$-quartz release study.[36] As can be seen in Fig. 7, the weighted fit to this functional form provides a reasonably good description of the experimentally determined $\Gamma_{\text{eff}}$. Also shown in the figure are the one-sigma uncertainty bands, which take into account the correlation of the uncertainty in the parameters from the weighted fit. The best fit values and the covariance

15

TABLE VIII. $\Gamma_{\text{eff}}$ for the TPX release experiments. $u_p^{\text{al}}$, $U_s^{\text{TPX}}$, and $\rho_0^{\text{TPX}}$ are the measured particle velocity of the aluminum (half the measured impact velocity), the measured shock velocity of the TPX samples, and the measured TPX initial density, respectively. $\Gamma_{\text{eff}}$ is the inferred value of the effective $\Gamma$ for the MGLR model. $u_p^{\text{IM}}$ is the inferred particle velocity in the shocked TPX determined from the MGLR model as described in Sec. IV.

| Expt | $u_p^{\text{al}}$ (km/s) | $U_s^{\text{TPX}}$ (km/s) | $\rho_0^{\text{TPX}}$ (g/cc) | $\Gamma_{\text{eff}}$ | $u_p^{\text{IM}}$ (km/s) |
|---|---|---|---|---|---|
| Z2450N | $8.86 \pm 0.03$ | $18.72 \pm 0.03$ | $0.83 \pm 0.004$ | $1.425 \pm 0.087$ | $12.26 \pm 0.06$ |
| Z2450S | $9.75 \pm 0.03$ | $20.21 \pm 0.03$ | $0.83 \pm 0.004$ | $1.343 \pm 0.072$ | $13.42 \pm 0.05$ |
| Z2345N | $11.97 \pm 0.03$ | $23.99 \pm 0.03$ | $0.83 \pm 0.004$ | $1.246 \pm 0.055$ | $16.26 \pm 0.05$ |
| Z2345S | $12.98 \pm 0.03$ | $25.68 \pm 0.03$ | $0.83 \pm 0.004$ | $1.192 \pm 0.047$ | $17.55 \pm 0.05$ |
| Z2333N | $12.98 \pm 0.03$ | $25.73 \pm 0.03$ | $0.83 \pm 0.004$ | $1.231 \pm 0.049$ | $17.54 \pm 0.05$ |
| Z2333S | $13.82 \pm 0.03$ | $27.04 \pm 0.03$ | $0.83 \pm 0.004$ | $1.121 \pm 0.044$ | $18.62 \pm 0.06$ |
| Z2375 | $15.80 \pm 0.07$ | $30.31 \pm 0.03$ | $0.83 \pm 0.004$ | $1.035 \pm 0.074$ | $21.13 \pm 0.13$ |

matrix elements are listed in Table XI.

We caution the use of this model outside of the range of the experimental data, specifically for $u_p^{\text{al}}$ below and above $\sim 9$ and $\sim 17$ km/s, respectively. This is particularly true for $u_p^{\text{al}}$ below $\sim 9$ km/s, where there is no data and it is unclear how best to extrapolate. Because both $S$ and $\Gamma_{\text{eff}}$ seem to asymptote at high $P$, one could likely use this fit for $u_p^{\text{al}}$ above $\sim 17$ km/s with some confidence. At $P$ above this limit, roughly 1200 GPa, $S$ asymptotes to the actual Hugoniot slope and $\Gamma_{\text{eff}}$ approaches a value close to what one would expect for an ideal gas.

## IV. ANALYTICAL RELEASE MODEL

As examples of this analytical release model, and as a consistency check, this IM method was used to determine the shocked states of the release standards for all of the aluminum release measurements listed in Tables VIII-X. Measurement of $u_p^{\text{al}}$ (in this case directly through impact velocity measurements, but could also be inferred through measured $U_s^{\text{al}}$ and

16

TABLE IX. $\Gamma_{\text{eff}}$ for the ~190 mg/cc silica aerogel release experiments. $u_p^{\text{al}}$, $U_s^{\text{gel}}$, and $\rho_0^{\text{gel}}$ are the measured particle velocity of the aluminum (half the measured impact velocity), the measured shock velocity of the aerogel samples, and the measured aerogel initial density, respectively. $\Gamma_{\text{eff}}$ is the inferred value of the effective $\Gamma$ for the MGLR model. $u_p^{\text{IM}}$ is the inferred particle velocity in the shocked aerogel determined from the MGLR model as described in Sec. IV.

| Expt | $u_p^{\text{al}}$ (km/s) | $U_s^{\text{gel}}$ (km/s) | $\rho_0^{\text{gel}}$ (mg/cc) | $\Gamma_{\text{eff}}$ | $u_p^{\text{IM}}$ (km/s) |
|---|---|---|---|---|---|
| Z1452 | $11.91 \pm 0.07$ | $25.45 \pm 0.14$ | $202 \pm 4$ | $1.138 \pm 0.165$ | $20.82 \pm 0.15$ |
| Z1474 | $12.86 \pm 0.07$ | $27.68 \pm 0.14$ | $197 \pm 4$ | $1.236 \pm 0.171$ | $22.42 \pm 0.16$ |
| Z1421 | $13.38 \pm 0.07$ | $28.65 \pm 0.14$ | $202 \pm 4$ | $1.203 \pm 0.154$ | $23.20 \pm 0.16$ |
| Z1472 | $13.55 \pm 0.07$ | $28.99 \pm 0.14$ | $203 \pm 4$ | $1.203 \pm 0.153$ | $23.46 \pm 0.16$ |
| Z1473 | $14.00 \pm 0.07$ | $29.71 \pm 0.14$ | $200 \pm 4$ | $1.033 \pm 0.124$ | $24.27 \pm 0.16$ |
| Z1451 | $14.35 \pm 0.07$ | $30.71 \pm 0.14$ | $202 \pm 4$ | $1.203 \pm 0.142$ | $24.76 \pm 0.16$ |
| Z1490 | $16.85 \pm 0.15$ | $35.45 \pm 0.25$ | $201 \pm 4$ | $0.947 \pm 0.163$ | $28.94 \pm 0.31$ |

TABLE X. $\Gamma_{\text{eff}}$ for the ~110 mg/cc silica aerogel release experiments. $u_p^{\text{al}}$, $U_s^{\text{gel}}$, and $\rho_0^{\text{gel}}$ are the measured particle velocity of the aluminum (half the measured impact velocity), the measured shock velocity of the aerogel samples, and the measured aerogel initial density, respectively. $\Gamma_{\text{eff}}$ is the inferred value of the effective $\Gamma$ for the MGLR model. $u_p^{\text{IM}}$ is the inferred particle velocity in the shocked aerogel determined from the MGLR model as described in Sec. IV.

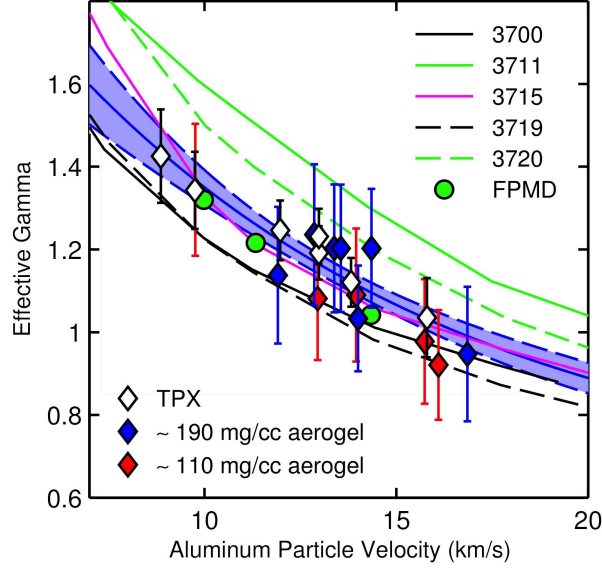| Expt | $u_p^{\text{al}}$ (km/s) | $U_s^{\text{gel}}$ (km/s) | $\rho_0^{\text{gel}}$ (mg/cc) | $\Gamma_{\text{eff}}$ | $u_p^{\text{IM}}$ (km/s) |
|---|---|---|---|---|---|
| Z2450S | $9.76 \pm 0.03$ | $22.16 \pm 0.06$ | $107 \pm 6$ | $1.353 \pm 0.136$ | $18.59 \pm 0.12$ |
| Z2333N | $12.95 \pm 0.03$ | $29.03 \pm 0.06$ | $111 \pm 6$ | $1.084 \pm 0.108$ | $24.21 \pm 0.16$ |
| Z2333S | $13.95 \pm 0.03$ | $31.3 \pm 0.06$ | $111 \pm 6$ | $1.092 \pm 0.114$ | $25.97 \pm 0.18$ |
| Z2375 | $15.74 \pm 0.07$ | $35.25 \pm 0.06$ | $107 \pm 6$ | $0.978 \pm 0.106$ | $29.36 \pm 0.25$ |
| Z2332 | $16.10 \pm 0.07$ | $35.88 \pm 0.06$ | $108 \pm 6$ | $0.921 \pm 0.103$ | $29.94 \pm 0.25$ |

FIG. 7. $\Gamma_{\text{eff}}$ as a function of the aluminum particle velocity along the Hugoniot, $u_p^{\text{al}}$. Open diamonds, TPX release measurements; blue (red) diamonds, $\sim$190 ($\sim$110) mg/cc silica aerogel release measurements; green circles, FPMD release calculations; black solid (dashed) line, 3700 (3719) EOS; green solid (dashed) line, 3711 (3720) EOS; magenta solid line, 3715 EOS; blue solid (dashed) line, best fit (one sigma deviation) to the experimental data.

TABLE XI. Fit parameters and covariance matrix elements for $\Gamma_{\text{eff}}(u_p^{\text{al}})$ [Eq. (4)].

| $a_1$ | $a_2$ | $a_3$ | $\sigma_{a_2}^2$ | $\sigma_{a_3}^2$ | $\sigma_{a_2}\sigma_{a_3}$ |
|---|---|---|---|---|---|
| | | $(\text{km/s})^{-1}$ | $(\times 10^{-2})$ | $(\times 10^{-4})$ | $(\times 10^{-3})$ |
| 0.6 | 1.942 | 0.0951 | 6.882 | 1.167 | 2.793 |

the known aluminum Hugoniot) determines $(i)$ the Hugoniot state of the aluminum, and thus $(P_1, u_{p1})$ from which the release path emanates, $(ii)$ the value of $S_1$ and therefore $C_{01}$ that defines the Hugoniot reference curve for the MGLR model [Eqs. (3) and (1), respectively], and $(iii)$ the value of $\Gamma_{\text{eff}}$ [Eq. (4)]. One then solves a set of coupled ordinary differential equations (ODEs), as described in detail in Ref. 36, to determine $(P, u_p)$ along the release path emanating from $(P_1, u_{p1})$. $P_1^{\text{sample}}$ and $u_{p1}^{\text{sample}}$ in the shocked state of the sample material are then determined by the intersection of $(P, u_p)$ along the release path and the chord defined by $P = (\rho_0^{\text{sample}} U_s^{\text{sample}})u_p$.

For each series of IM calculations the coefficients of the aluminum Hugoniot are sampled

18

within their uncertainty defined by the covariance matrix (Table I). This propagates the uncertainty in the initial state $(P_1, u_{p1})$ as well as uncertainties in $S_1$ and $C_{01}$. Then for each IM calculation in the series of measurements, $u_p^{\text{al}}$, $\Gamma_{\text{eff}}$, $U_s^{\text{sample}}$, and $\rho_0^{\text{sample}}$ are all sampled within their one-sigma uncertainty. $(P_1^{\text{sample}}, u_{p1}^{\text{sample}})$ is then determined as the intersection of the chord and release path, and the remaining kinematic variables can be evaluated through the use of the Rankine-Hugoniot jump conditions.[34] This process is repeated for $10^6$ iterations, and the reported values and one-sigma uncertainties of the inferred quantities are taken to be the mean and standard deviations of the Monte Carlo distributions, respectively.

The resulting $U_s - u_p$ points from the IM method using the analytical release model (the inferred $u_p$ are listed in the last column of Tables VIII-X) are in excellent agreement with the direct impact results.[44,45,59] This provides a consistency check, and indicates that the assumptions of the analytical model, namely that $\Gamma_{\text{eff}}$ can be treated as a constant regardless of the impedance of the unknown material, is justified. Furthermore, the uncertainty in the inferred $u_p$ is roughly equivalent for both the analytical IM release model and for the direct impact experiments. This suggests that there is very little loss in precision or accuracy in using aluminum as an IM standard as opposed to performing direct impact experiments with aluminum. This is significant in that impact type experiments in the multimegabar regime are currently limited to explosively driven striker plate and magnetically driven flyer plate platforms.

As a final example we discuss previously published laser driven Hugoniot experiments on deuterium reported by Hicks $et$ $al.$[20] In that study, a laser driven shock in aluminum was driven into both a liquid deuterium sample and an $\alpha$-quartz sample used to better determine the shocked state of the aluminum drive plate. To perform the IM analysis, an experimentally determined mapping was used to infer the shocked state of the aluminum from the measured $U_s^{\text{q}}$. The inferred $U_s^{\text{al}}$ along with a fit of available absolute Hugoniot data for aluminum then defined $(P_1, u_{p1})$ of the shocked aluminum. The release response was then determined through a model developed by comparing the difference between the RH and the calculated release response of several different tabular EOS models from aluminum, as described in Ref. 20.

For this reanalysis we take advantage of the recent, significant improvement in precision of the $\alpha$-quartz Hugoniot[36,60] and the present aluminum release model. In particular, we used the measured $U_s^{\text{q}}$ and the known $\alpha$-quartz Hugoniot[36,60] to define a point $(P_{\text{q}}, u_p^{\text{q}})$
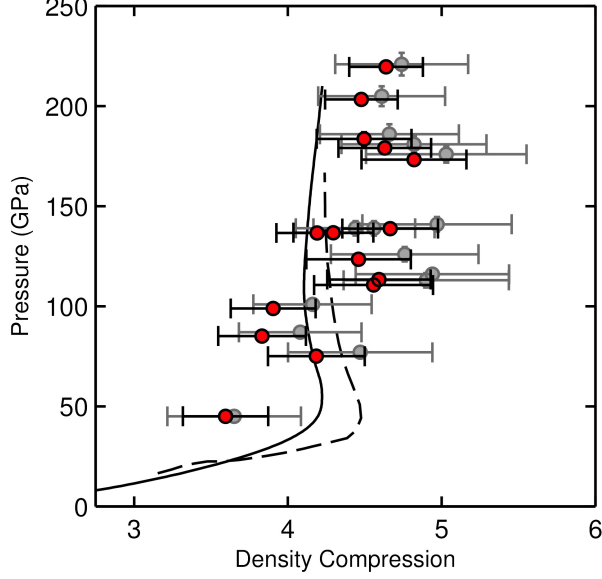
FIG. 8. $P$ - $\rho/\rho_0$ Hugoniot for laser driven deuterium experiments.[20] Black solid (dashed) line, Hugoniot from the Kerley03 EOS[61] (Holst FPMD[62]). Gray circles, Hugoniot data as published in Ref. 20; red circles, this reanalysis.

through which the aluminum release must pass through. To do this we first reconstructed the measured $U_s^q$ in Ref. 20 from the reported $U_s^{al}$ by inverting the relationship between $U_s^{al}$ and $U_s^q$:

$$U_s^q = \beta + \left(U_s^{al} - a_0\right)/a_1, \tag{5}$$

$$\delta U_s^q = \frac{\left[\left[\left(\delta U_s^{al}\right)^2 - \sigma_{a0}^2\right] - \left(U_s^q - \beta\right)^2 \sigma_{a1}^2\right]^{1/2}}{a_1}, \tag{6}$$

where $\beta = 20.57$, $a_0 = 21.14$ km/s, $a_1 = 0.91$, $\sigma_{a0} = 0.12$, and $\sigma_{a1} = 0.03$. The resulting values of $U_s^q$ and $\delta U_s^q$ are listed in Table XII.

For each experiment we then used the MGLR model to determine $(P_1, u_{p1})$ for the shocked state of aluminum such that the release path passed through $(P_q, u_p^q)$ determined from the measured $U_s^q$. The intersection of this release path with the chord defined by $P = (\rho_0^{D2} U_s^{D2})u_p$ then provided $(P_{D2}, u_p^{D2})$. The remaining kinematic variables for the deuterium were determined using the Rankine-Hugoniot relations.[34] The inferred values from this reanalysis are listed in Table XII and displayed in Fig. 8.

As can be seen in Table XII and Fig. 8, the reanalysis results in a systemically lower density compression with respect to the published values.[20] This is predominantly due to the im-

20

TABLE XII. Comparison of the inferred $P$ and $\rho/\rho_0$ for laser driven experiments on deuterium using the aluminum IM method, as described in the text. The uncertainties in $P$ and $\rho/\rho_0$ from Ref. 20 list the random and systematic components of the uncertainties explicitly in parentheses: (ran, sys). The quadrature sum of these individual components of uncertainty are displayed in Fig. 8.

| Shot | $U_s^{\mathrm{al}}$ (km/s) | $U_s^{\mathrm{q}}$ (km/s) | $U_s^{\mathrm{D2}}$ (km/s) | Hicks et al.[20] | | this reanalysis | |
|---|---|---|---|---|---|---|---|
| | | | | $P$ (GPa) | $\rho/\rho_0$ | $P$ (GPa) | $\rho/\rho_0$ |
| 31700 | $26.07 \pm 0.34$ | $25.99 \pm 0.30$ | $36.87 \pm 0.33$ | $186 \pm (4,3)$ | $4.66 \pm (0.37, 0.26)$ | $184 \pm 3$ | $4.47 \pm 0.31$ |
| 31692 | $21.88 \pm 0.25$ | $21.38 \pm 0.24$ | $28.89 \pm 0.32$ | $116 \pm (2,2)$ | $4.94 \pm (0.42, 0.27)$ | $113 \pm 2$ | $4.56 \pm 0.34$ |
| 31912 | $18.75 \pm 0.25$ | $17.94 \pm 0.22$ | $23.83 \pm 0.32$ | $77 \pm (2,1)$ | $4.47 \pm (0.42, 0.21)$ | $75 \pm 2$ | $4.16 \pm 0.32$ |
| 31910 | $15.51 \pm 0.31$ | $14.38 \pm 0.24$ | $18.96 \pm 0.31$ | $45 \pm (2,1)$ | $3.65 \pm (0.40, 0.17)$ | $45 \pm 1$ | $3.57 \pm 0.28$ |
| 32248 | $23.30 \pm 0.25$ | $22.94 \pm 0.23$ | $32.03 \pm 0.32$ | $139 \pm (3,2)$ | $4.56 \pm (0.32, 0.23)$ | $137 \pm 2$ | $4.28 \pm 0.26$ |
| 32252 | $25.65 \pm 0.29$ | $25.53 \pm 0.24$ | $35.48 \pm 0.39$ | $176 \pm (3,3)$ | $5.03 \pm (0.42, 0.31)$ | $173 \pm 3$ | $4.79 \pm 0.34$ |
| 32254 | $27.08 \pm 0.31$ | $27.10 \pm 0.23$ | $38.81 \pm 0.31$ | $205 \pm (4,3)$ | $4.61 \pm (0.32, 0.26)$ | $203 \pm 3$ | $4.46 \pm 0.24$ |
| 32258 | $27.96 \pm 0.32$ | $28.06 \pm 0.21$ | $40.13 \pm 0.31$ | $221 \pm (4,4)$ | $4.74 \pm (0.33, 0.28)$ | $220 \pm 3$ | $4.63 \pm 0.24$ |
| 32864 | $19.45 \pm 0.29$ | $18.71 \pm 0.28$ | $25.76 \pm 0.34$ | $87 \pm (2,1)$ | $4.07 \pm (0.36, 0.17)$ | $85 \pm 2$ | $3.81 \pm 0.29$ |
| 32866 | $21.67 \pm 0.27$ | $21.15 \pm 0.27$ | $28.57 \pm 0.39$ | $113 \pm (3,2)$ | $4.90 \pm (0.47, 0.26)$ | $111 \pm 2$ | $4.52 \pm 0.39$ |
| 33190 | $25.89 \pm 0.31$ | $25.79 \pm 0.26$ | $36.26 \pm 0.34$ | $181 \pm (3,3)$ | $4.82 \pm (0.38, 0.28)$ | $179 \pm 3$ | $4.61 \pm 0.30$ |
| 33194 | $23.24 \pm 0.27$ | $22.88 \pm 0.25$ | $32.14 \pm 0.34$ | $139 \pm (3,2)$ | $4.44 \pm (0.32, 0.22)$ | $137 \pm 3$ | $4.17 \pm 0.27$ |
| 34135 | $20.55 \pm 0.28$ | $19.92 \pm 0.28$ | $27.67 \pm 0.34$ | $101 \pm (2,1)$ | $4.16 \pm (0.34, 0.18)$ | $99 \pm 2$ | $3.88 \pm 0.28$ |
| 34139 | $23.58 \pm 0.26$ | $23.25 \pm 0.24$ | $31.89 \pm 0.31$ | $141 \pm (3,2)$ | $4.97 \pm (0.39, 0.29)$ | $139 \pm 2$ | $4.64 \pm 0.31$ |
| 34144 | $22.51 \pm 0.27$ | $22.08 \pm 0.26$ | $30.27 \pm 0.37$ | $126 \pm (3,2)$ | $4.76 \pm (0.41, 0.25)$ | $123 \pm 2$ | $4.43 \pm 0.34$ |

proved description of the $\alpha$-quartz Hugoniot; the recently published $\alpha$-quartz Hugoniot[36,60] is significantly less compressible than the effective Hugoniot used in Ref. 20 (linear mapping relating $U_s^{\mathrm{q}}$ to $U_s^{\mathrm{al}}$), resulting in lower inferred density compression for the deuterium. A close comparison of Fig. 5 from Ref. 60, which essentially only corrected for the difference in the $\alpha$-quartz Hugoniot, with Fig. 8 from the present work shows that the effect of the present aluminum release model somewhat compensates for this error. This would indicate that the present aluminum release model results in systematically slightly higher inferred $u_p$ along the release path when compared to the release model used in Ref. 60, which was based mainly on the difference between the release path and the RH for the 3700 EOS model, in accordance with a previous aluminum release study.[43] This difference is consistent with

Fig. 7 in that the best fit trend line of the experimentally determined $\Gamma_{\text{eff}}$ is systematically higher than that determined from the 3700 EOS table, which would result in a slightly higher inferred $u_p$ along the aluminum release path and therefore a slightly higher inferred $\rho/\rho_0$ for deuterium.

More significantly, comparison of the two analyses displayed in Fig. 8 demonstrates that the uncertainty in the inferred shock state is significantly smaller for the MGLR analysis as compared to the analysis used in Ref. 20. This is undoubtably due to experimental constraint on the release behavior from this work. With little direct experimental guidance, Hicks *et al.* were forced to resort to examination of various EOS models in an attempt to constrain the release behavior of aluminum, with resultantly large contributions from potential systematic uncertainty (note the large systematic spread in $\Gamma_{\text{eff}}$ between the various tabular EOS models displayed in Fig. 7). The experiments described in Sec. III enabled a determination of $\Gamma_{\text{eff}}$ with relatively tight constraint. As a result, the inferred quantities, particularly $\rho/\rho_0$, exhibit significantly lower uncertainty, thereby increasing the precision of the IM method with aluminum as the standard.


## V.   CONCLUSION

The release response of aluminum was investigated within the framework of first-principles molecular dynamics (FPMD) and several tabular equation of state (EOS) models for aluminum. These calculations provided insight into the release response of aluminum, and motivated a simple Mie-Grüneisen model with a linear $U_s - u_p$ Hugoniot as the reference, referred to as the MGLR model. This model was shown to reproduce the FPMD and tabular EOS release paths extremely well with a constant $\Gamma_{\text{eff}}$ along the release path, with both $S$, the slope of the Hugoniot reference for the MG model, and $\Gamma_{\text{eff}}$ being functions of $u_p^{\text{al}}$ [see Eqs. (3) and (4)].

A series of plate impact, shock wave experiments were performed on the Sandia Z machine to obtain release data for aluminum from $\sim$400-1200 GPa states on the principal Hugoniot. Three different low-impedance standards were used, TPX, $\sim$190 and $\sim$110 mg/cc silica aerogel, which vary in shock impedance by roughly an order of magnitude. These data validated the MGLR model that was motivated by the FPMD and tabular EOS study, and provided an experimentally determined $\Gamma_{\text{eff}}$ as a function of $u_p^{\text{al}}$.

22

This theoretical and experimental study of the release response of aluminum provides a simple, analytical model for performing IM calculations without the need to appeal to any particular tabular EOS for aluminum. Since the model is analytical, it is well suited for the use of Monte Carlo analysis methods, enabling all uncertainty, including the random measurement uncertainty and any systematic uncertainty in the Hugoniot and release response of aluminum, to be propagated to the inferred quantities. We also note that the experimentally validated model framework should prove to be useful in the development of wide range equations of state for aluminum, in that it constrains the kinematic variables of aluminum upon release over a wide range of $P$ and $\rho$.

It is emphasized that the MGLR model discussed here is only intended to calculate kinematic variables for aluminum upon release, in particular the release paths in the $P - u_p$ plane for purposes of impedance matching. It is fully expected that other aspects of the MGLR model will be incorrect. In particular, it is anticipated that the temperatures and specific heats of the MGLR model do not reflect the behavior of aluminum in this regime. Furthermore, we caution the use of this model outside of the range of the experimental data, specifically for $u_p^{\mathrm{al}}$ below and above $\sim$9 and $\sim$17 km/s, respectively. This is particularly true for $u_p^{\mathrm{al}}$ below $\sim$9 km/s, where there is no data and it is unclear how best to extrapolate. Because both $S$ and $\Gamma_{\mathrm{eff}}$ seem to asymptote at high $P$, one could likely use this fit for $u_p^{\mathrm{al}}$ above $\sim$17 km/s with some confidence. At $P$ above this limit, roughly 1200 GPa, $S$ asymptotes to the actual Hugoniot slope and $\Gamma_{\mathrm{eff}}$ approaches a value close to what one would expect for an ideal gas.

As an example of its use, the MGLR model was used to infer Hugoniot states through the IM method for all of the aluminum release measurements performed for this study. This provided a consistency check in that the IM results could be compared to the direct impact Hugoniot measurements of the standards. Not only did the IM Hugoniot response agree extremely well with the direct impact Hugoniot results, but the uncertainties from the two methods were found to be roughly equivalent. This suggests that the IM method can confidently be used to obtain high-precision Hugoniot measurements regardless of the shock impedance of the unknown material. In particular, given the prolific use of aluminum as an IM standard, the present IM model will enable reanalysis of numerous multimegabar experiments in the literature. Such reanalyses will improve both the accuracy and precision of the inferred shock response by taking advantage of recent refinement of the Hugoniot

response of aluminum, as well as an experimentally validated release model which tightly constrains the release response of aluminum in the multimegabar regime.

## ACKNOWLEDGMENTS

---

[*] mdknuds@sandia.gov

[1] T. Guillot, Science **286**, 72 (1999).

[2] I. Baraffe, G. Chabrier, and T. Barman, Astron. Astrophys. **482**, 315 (2008).

[3] J. Fortney and N. Nettelmann, Space Sci. Rev. **152**, 423 (2009).

[4] J. Lindl, *Inertial Confinement Fusion* (Springer, New York, 1998).

[5] J. Lindl, Phys. Plasmas **2**, 3933 (1995).

[6] R. G. McQueen, S. P. Marsh, J. W. Taylor, . N. Fritz, and W. J. Carter, "High velocity impact phenomena," (Academic, New York, 1970) p. 515.

[7] A. C. Mitchell and W. J. Nellis, J. Appl. Phys. **52**, 3363 (1981).

[8] W. J. Nellis, H. B. Radousky, D. C. Hamilton, A. C. Mitchall, N. C. Holmes, K. B. Christianson, and M. Thiel, J. Chem. Phys. **94**, 2244 (1991).

[9] L. V. Al'tshuler, S. B. Kormer, A. A. Bakanova, and R. F. Trunin, Zh. Eksp. Teor. Fiz. **38**, 790 (1960), [Sov. Phys.-JETP **11**, 573 (1960)].

[10] S. B. Kormer, A. I. Funtikov, V. D. Urlin, and A. N. Kolesnikova, Zh. Eksp. Teor. Fiz. **42**, 626 (1962), [Sov. Phys.-JETP **15**, 477 (1962)].

[11] B. L. Glushak, A. P. Zharkov, M. V. Zhernokletov, V. Y. Ternovoi, A. S. Filimonov, and V. E. Fortov, Zh. Eksp. Teor. Fiz. **96**, 1301 (1989), [Sov. Phys.-JETP **69**, 739 (1989)].

[12] S. I. Belov, G. V. Boriskov, A. I. Bykov, R. I. Il'kaev, N. B. Luk'yanov, A. Ya. Matveev, O. L.

24

Mikhailova, V. D. Selemir, G. V. Simakov, R. F. Trunin, I. P. Trusov, V. D. Urlin, V. E. Fortov, and A. N. Shuikin, Pis'ma Zh. Eksp. Teor. Fiz. **76**, 508 (2002), [JETP Lett. **76**, 433 (2002)].

[13] G. V. Boriskov, A. I. Bykov, R. I. Il'kaev, V. D. Selemir, G. V. Simakov, R. F. Trunin, V. D. Urlin, V. E. Fortov, and A. N. Shuikin, Dokl. Akad. Nauk. **392**, 755 (2003), [Dokl. Phys. **48**, 553 (2003)].

[14] G. V. Boriskov, A. I. Bykov, R. I. Il'kaev, V. D. Selemir, G. V. Simakov, R. F. Trunin, V. D. Urlin, A. N. Shuikin, and W. J. Nellis, Phys. Rev. B **71**, 092104 (2005).

[15] D. G. Hicks, P. M. Celliers, G. W. Collins, J. H. Eggert, and S. J. Moon, Phys. Rev. Lett. **91**, 035502 (2003).

[16] K. Takamatsu *et al.*, Phys. Rev. E **67**, 056406 (2003).

[17] P. M. Celliers *et al.*, Phys. Plasmas **11**, L41 (2004).

[18] D. G. Hicks, T. R. Boehly, P. M. Celliers, J. H. Eggert, E. Vianello, D. D. Meyerhofer, and G. W. Collins, Phys. Plasmas **12**, 082702 (2005).

[19] N. Ozaki *et al.*, Phys. Plasmas **12**, 124503 (2005).

[20] D. G. Hicks, T. R. Boehly, P. M. Celliers, J. H. Eggert, S. J. Moon, D. D. Meyerhofer, and G. W. Collins, Phys. Rev. B **79**, 014112 (2009).

[21] M. D. Knudson, R. W. Lemke, D. B. Hayes, C. A. Hall, C. Deeney, and J. R. Asay, J. Appl. Phys. **94**, 4420 (2003).

[22] R. Lemke, M. D. Knudson, A. Robinson, T. Haill, K. Struve, J. Asay, and T. Mehlhorn, Phys. Plasmas **10**, 1867 (2003).

[23] M. D. Knudson, D. L. Hanson, J. E. Bailey, C. A. Hall, J. R. Asay, and C. Deeney, Phys. Rev. B **69**, 144209 (2004).

[24] R. Lemke, M. D. Knudson, and J.-P. Davis, Int. J. Impact Eng. **38**, 480 (2011).

[25] M. D. Knudson, M. P. Desjarlais, R. W. Lemke, T. R. Mattsson, M. French, N. Nettelmann, and R. Redmer, Phys. Rev. Lett **108**, 091102 (2012).

[26] L. V. Al'tshuler, N. N. Kalitkin, L. V. Kuz'mina, and B. S. Chekin, Zh. Eksp. Teor. Fiz. **72**, 317 (1977), [Sov. Phys.-JETP **45**, 167 (1977)].

[27] L. P. Volkov, N. P. Voloshin, A. S. Vladimirov, V. N. Nogin, and V. A. Simonenko, Pis'ma Zh. Eksp. Teor. Fiz. **31**, 623 (1980), [JETP Lett. **31**, 588 (1980)].

[28] L. V. Al'tshuler, A. A. Bakanova, I. P. Dudoladov, E. A. Dynin, R. F. Trunin, and B. S. Chekin, J. Appl. Mech. Tech. Phys. **22**, 145 (1981).

[458] [29] C. E. Ragan, Phys. Rev. A **25**, 3360 (1982).

[459] [30] C. E. Ragan, Phys. Rev. A **29**, 1391 (1984).

[460] [31] V. A. Simonenko, N. P. Voloshin, A. S. Vladimirov, A. P. Nagibin, V. N. Nogin, V. A. Popov,
[461] V. A. Sal'nikov, and Y. A. Shoidin, Zh. Eksp. Teor. Fiz. **88**, 1452 (1985), [Sov. Phys.-JETP
[462] **61**, 869 (1985)].

[463] [32] A. C. Mitchell, W. J. Nellis, J. A. Moriarty, R. A. Heinle, N. C. Holmes, R. E. Tipton, and
[464] G. W. Repp, J. Appl. Phys. **69**, 2981 (1991).

[465] [33] L. V. Al'tshuler, K. K. Krupnikov, B. N. Ledenev, V. I. Zhuckikhin, and M. I. Brazhnik, Zh.
[466] Eksp. Teor. Fiz. **34**, 874 (1958), [Sov. Phys.-JETP **7**, 606 (1958)].

[467] [34] G. E. Duvall and R. A. Graham, Rev. Mod. Phys. **49**, 523 (1977).

[468] [35] S. Root, R. J. Magyar, J. H. Carpenter, D. L. Hanson, and T. R. Mattsson, Phys. Rev. Lett.
[469] **105**, 085501 (2010).

[470] [36] M. D. Knudson and M. P. Desjarlais, Phys. Rev. B **88**, 184107 (2013).

[471] [37] G. I. Kerley, Int. J. Impact Eng. **5**, 441 (1987).

[472] [38] G. Kerley, Kerley Publishing Services Report No. KPS98-1 (Kerley Publishing Services, 1998).

[473] [39] K. S. Holian, Lawrence Livermore National Laboratory Report No. UCID-118574-82-2
[474] (Lawrence Livermore National Laboratory, 1982).

[475] [40] K. S. Holian, Los Alamos National Laboratory Report No. LA-10160-MS (Los Alamos National
[476] Laboratory, 1984).

[477] [41] TFD variations due to D. Liberman, R. D. Cowan, and J. Ashkin, Phys. Rev. **105**, 144 (1957).

[478] [42] Nuclear variation of J. D. Johnson, High Press. Res. **6**, 277 (1991).

[479] [43] M. D. Knudson, J. R. Asay, and C. Deeney, J. Appl. Phys. **97**, 073514 (2005).

[480] [44] M. D. Knudson and R. W. Lemke, J. Appl. Phys. **114**, 053510 (2013).

[481] [45] S. Root (unpublished).

[482] [46] G. Kresse and J. Furthmüller, Phys. Rev. B **54**, 11169 (1996).

[483] [47] P. E. Blöchl, Phys. Rev. B **50**, 17953 (1994).

[484] [48] G. Kresse and D. Joubert, Phys. Rev. B **59**, 1758 (1999).

[485] [49] J. P. Perdew, K. Burke, and M. Ernzerhof, Phys. Rev. Lett. **77**, 3865 (1996).

[486] [50] A. Baldereschi, Phys. Rev. B **7**, 5212 (1973).

[487] [51] M. D. Knudson (unpublished).

[488] [52] M. Matzen *et al.*, Phys. Plasmas **12**, 055503 (2005).

[489] [53] L. M. Barker and R. E. Hollenbach, J. Appl. Phys. **43**, 4669 (1972).

[490] [54] from manufacturers website: http://www.mitsuichemicals.com/tpx.htm.

[491] [55] A. Danilyuk *et al.*, Nucl. Instr. and Meth. A **494**, 491 (2002).

[492] [56] D. Richter and D. Lipka, Nucl. Instr. and Meth. A **513**, 635 (2003).

[493] [57] S. L. Thompson, Sandia National Laboratories Report No. SAND89-2951 (Sandia National
[494] Laboratories, 1990).

[495] [58] S. D. Crockett, Los Alamos National Laboratory Report No. LA-UR-04-6442 (Los Alamos
[496] National Laboratory, 2004).

[497] [59] We did not display a comparison of the $U_s - u_p$ results from the IM analysis and the direct
[498] impact experiments as they look very similar to Figs. 9-11 in Ref. 36.

[499] [60] M. D. Knudson and M. P. Desjarlais, Phys. Rev. Lett **103**, 225501 (2009).

[500] [61] G. Kerley, Sandia National Laboratories Report No. SAND2003-3613 (Sandia National Labo-
[501] ratories, 2003).

[502] [62] B. Holst, R. Redmer, and M. P. Desjarlais, Phys. Rev. B **77**, 184201 (2008).